Environmental Fluid Mechanics **1:** 29–47, 2001.

Large-Eddy Simulations of the Atmospheric Boundary Layer Using a New Subgrid-Scale Model

I. *Slightly unstable and neutral cases*

FENG DING, S. PAL ARYA and YUH-LANG LIN
Department of marine, Earth and Atmospheric Sciences, North Carolina State University, Raleigh, NC 27695-8208, U.S.A.

Received 14 August 2000; accepted in revised form 5 October 2000

Abstract. Subgrid-scale (SGS) modeling is a long-standing problem and a critical component in the large-eddy simulation (LES) of atmospheric boundary layer. A variety of SGS models with different levels of sophistication have been proposed for different needs, such as Smagorinsky's (1963) eddy viscosity model, Mason and Thomson's (1992) stochastic backscattering model, and Sullivan *et al.*'s (1994) near surface model. A modified Smagorinsky SGS model has been used in the LES version of Terminal Area Simulation System (TASS-LES). It has successfully simulated the buoyancy-dominated, convective atmospheric boundary layer flows, while simulations of the shear-dominated, slightly unstable, neutral, and stably stratified boundary layer flows are not so good. For the later, we used a simpler version of Sullivan *et al.*'s subgrid-scale model in which turbulent kinetic energy equation is not included and the model is still the first-order closure. A momentum profile matching approach is adopted in the proposed model. A series of simulations for shear-dominated, slightly unstable and neutral boundary layers are performed using different subgrid-scale models and different grid resolutions. The results are compared with those of Sullivan *et al.* (1994) and with empirical similarity relations for the surface layer. The simulations with the new SGS model appear to be far more satisfactory than those with the modified Smagorinsky model.

1. Introduction

The application of large-eddy simulation (LES) to atmospheric boundary layer (ABL) modeling started with Deardorff's (1970, 1973) pioneering work in early seventies (Arya, 1999). It is still the best available approach to atmospheric turbulence and diffusion modeling. In LES only large energy-containing eddies, which are responsible for most turbulent transports of momentum, heat and mass in the flow, are explicitly resolved. It is accomplished by filtering-out the high-frequency component of the flow field and using the low-pass-filtered form of Navier–Stokes equations to solve for the large-scale component only (Kosovic, 1997). The effects of the filtered-out small-scale fields on the resolved fields are then parameterized. These parameterizations constitute the so-called subgrid-scale (SGS) model.

SGS model is a critical component for any successful LES, and also a long-standing problem in LES. This is because all SGS models contain some uncertainties and errors arising from the simplifying assumptions and closure hypotheses used in the SGS parameterizations. A number of SGS models have been proposed in the past with different levels of sophistication for different needs and

requirements. Most of them are first-order closure models with or without the SGS turbulence kinetic energy (TKE) equation; higher-order closure models are rarely used in LES of ABL due to their large computational cost. Probably the simplest and the most widely used SGS model is the Smagorinsky model (Smagorinsky, 1963), which was originally used in an atmospheric general circulation model, and was based on the SGS eddy viscosity or gradient-transport concept. Simple modifications of the Smagorinsky's model to include the effects of stability are often used. More refined models use a turbulence kinetic energy closure scheme to express the SGS eddy viscosity (see, e.g., Moeng, 1984; Nieuwstadt and Brost, 1986; Mason, 1989).

Mason (1994) presented a critical review of LES technique and its related SGS models. He pointed out that the weakest part of a LES is the SGS modeling near the surface and in stably stratified regions where turbulence scales became small in relation to the scale of the filter. In such regions an empirical approach has been used in which the SGS closure represents stochastic fluctuations of the unresolved stress. Mason and Thomson (1992) developed the stochastic backscattering SGS model which accounts for the stochastic effects resulting in the backscattering of energy. Andren *et al.* (1994) compared the simulation results from different models. It was shown that the SGS model incorporating stochastic backscattering of energy gave much better results, albeit at higher computational cost, than those without stochastic backscattering for the same grid resolutions.

Sullivan *et al.* (1994) formulated a two-part eddy viscosity SGS model based on Moeng's (1984) TKE closure model. The concept of two-part eddy viscosity was first proposed by Schuman (1975). In this SGS model, eddy viscosity is separated into a mean-field part and a fluctuating part, and the equations for computing mean-field eddy viscosity are based on the surface layer similarity theory. In the two-part eddy viscosity model, the computation of SGS stress is split into isotropic and inhomogeneous contributions. Sullivan *et al.* (1994) defined an isotropy factor as the ratio of horizontal-averaged fluctuating resolved strain to the sum of itself and horizontal-averaged mean resolved strain. This isotropy factor was used as the weighting parameter to determine the inhomogeneous SGS stress part and to make a smooth transition between their two-part eddy viscosity model and baseline TKE closure model. The simulation of near-neutral boundary layer with this model clearly showed logarithmic profiles near the surface for both the wind speed and potential temperature. Andren (1995) used the same SGS model for weakly stable boundary layers and showed that the SGS model of Sullivan *et al.* (1994) was about as successful in improving the near-surface behavior as computationally more expensive stochastic backscattering model. In both models, the importance of inhomogeneous turbulence near the bounding surfaces is recognized and mean profiles obtained show good agreement with their empirical forms based on the Monin-Obukhov similarity theory in the surface layer.

Recently, Kosovic (1997) has argued that SGS models must capture inertial transfer effects including the backscattering of energy as well as its redistribution

among the normal SGS stress components. These effects are a consequence of nonlinear interactions and anisotropy. He developed a nonlinear SGS model capable of reproducing the effects of SGS anisotropic characteristic of shear-driven boundary layers. Since many more terms are involved in the nonlinear model than in a linear two-part eddy viscosity model, Kosovic's model is computationally more demanding and expensive. It has also been shown to work only under neutral and stable conditions and not under buoyancy-dominated unstable and convective conditions.

In our large-eddy simulations of the ABL, we have utilized a new SGS model which is an extension of that proposed by Sullivan *et al.* (1994). The proposed SGS model is based on their two-part eddy viscosity model and the same expression for mean-field eddy viscosity at the first grid level (z_1) is used. However, a different expression based on the SGS momentum flux profile is derived for the grid levels above z_1. This model is incorporated in the LES version of Terminal Area Simulation System (TASS) for simulations of shear-dominated weakly unstable and neutral atmospheric boundary layers. The results are compared with other first-order SGS models, as well as the surface layer similarity relations.

2. Subgrid-Scale Models

2.1. MODIFIED SMAGORINSKY SGS MODEL

The TASS was originally developed by Proctor (1987) for the study of thunderstorms and microbursts (Proctor, 1988). After some modifications, it became a LES model for the simulation of the ABL (Schowalter *et al.*, 1995, 1996). It uses nonhydrostatic and compressible forms of conservation equations. The condensation and precipitation are not allowed in the present simulations.

A modified Smagorinsky first-order closure is used, and the expression for the subgrid scale turbulent stress is:

$$\tau_{ij} = \rho_0 K_M D_{ij} = \rho_0 K_M \left(\frac{\partial U_i}{\partial x_j} + \frac{\partial U_j}{\partial x_i} - \frac{2}{3} \frac{\partial U_k}{\partial x_k} \delta_{ij} \right), \tag{1}$$

where τ_{ij} is the subgrid scale turbulent stress tensor, ρ_0 the density of the environment, K_M the SGS eddy viscosity for momentum, U_i the velocity components of the resolved flow, and D_{ij} the deformation tensor which represents the terms inside the parentheses in Equation (1). A similar expression is used for the subgrid scale heat flux:

$$S_{j\theta} = -c_p \rho_0 K_H \frac{\partial \Theta}{\partial x_j}, \tag{2}$$

here, Θ is the potential temperature and K_H is the SGS eddy diffusivity of heat. Following Deardorff (1973), a constant diffusivity ratio $K_H/K_M = 3$ has been used.

Eddy viscosity K_M is taken proportional to the square of mixing length and also depends on the deformation and stability as:

$$K_M = l^2 \sqrt{\tfrac{1}{2} D_{ij} D_{ij} \left(1 - R_f\right)} = l^2 \sqrt{2\, S_{ij}\, S_{ij} \left(1 - R_f\right)}, \tag{3}$$

where l is the SGS mixing length, $S_{ij} = D_{ij}/\,2$ is the strain rate tensor, and R_f is the local flux Richardson number. Following Mason (1994), l is expressed as:

$$l = \alpha \Delta \qquad kz \geqslant \alpha \Delta, \tag{4}$$

$$l = \frac{\alpha \Delta \left[1 + (\alpha \Delta / kz)^{n-1}\right]}{1 + (\alpha \Delta / kz)^n} \qquad \alpha \Delta > kz > k \Delta z/2, \tag{5}$$

$$l = kz \qquad kz \leqslant k \Delta z/2, \tag{6}$$

$$\Delta = (2 \Delta x 2 \Delta y 2 \Delta z)^{1/3}, \tag{7}$$

here α is an empirical constant, k is the von Karmán constant, and Δ is the geometric average grid mesh spacing. The purpose of Equations (4) and (5) is to match the mixing length to the appropriate value close to the ground where flow is under-resolved. The matching parameter n is set to 2.5. Equations (4)–(6) are used in TASS-LES; together with Equations (1)–(3), they constitute the modified Smagorinski SGS model.

2.2. SIMPLIFIED TWO-PART EDDY VISCOSITY MODEL

The TASS-LES model has successfully simulated ABLs under unstable and convective conditions (Schowalter *et al.*, 1995, 1996; DeCroix *et al.*, 1997). But the results from the simulations of weakly unstable and neutral boundary layer flows are found to be somewhat inferior. The model overestimates mean wind shear in the surface layer and lower part of the ABL.

In order to get better results in the surface layer and lower part of the ABL, a simplified version of Sullivan *et al.*'s (1994) two-part eddy viscosity SGS model was also utilized in the TASS-LES model. We used their expression for the SGS momentum flux tensor:

$$F_{ij} = -2\gamma \nu_t S_{ij} - 2\nu_T \langle S_{ij} \rangle, \tag{8}$$

where $F_{ij} = -\tau_{ij} / \rho_0$. Here the angle brackets denote averages over the horizontal planes, ν_t and ν_T are fluctuating and mean-field turbulent eddy viscosities respectively, S_{ij} is the strain rate tensor for the resolved flow, and γ is an isotropy factor defined as:

$$\gamma = \frac{S'}{S' + \langle S \rangle}, \tag{9}$$

where

$$\langle S \rangle = \sqrt{2\langle S_{ij} \rangle \langle S_{ij} \rangle}, \tag{10}$$

and

$$S' = \sqrt{2\langle \left(S_{ij} - \langle S_{ij} \rangle\right)\left(S_{ij} - \langle S_{ij} \rangle\right) \rangle}. \tag{11}$$

The isotropy factor γ is expected to increase with height and approach unity at the top of the PBL.

The same modified Smagorinsky expression is still used to compute ν_t as that used for K_M in Equation (3):

$$\nu_t = l^2 \left[\left(2S_{ij}S_{ij}\right)\left(1 - R_f\right)\right]^{1/2}. \tag{12}$$

For the mean-field eddy viscosity at the first grid point height z_1, Sullivan *et al.* (1994) derived the following expression, assuming that z_1 falls within the constant flux surface layer:

$$\nu_T^* = \frac{u_* k z_1}{\phi_m(z_1)} - \langle \nu_t \gamma \rangle - \frac{k z_1}{u_* \phi_m(z_1)} \left[\langle uw \rangle^2 + \langle vw \rangle^2\right]^{1/2}, \tag{13}$$

where $\phi_m(z_1)$ is the dimensionless wind shear at $z = z_1$, which can be expressed in terms of Monin–Obukhov similarity relations. At other heights $z > z_1$, they assumed

$$\nu_T = \nu_T^* \frac{k z_1}{u_* \phi_m(z_1)} \sqrt{2\langle S_{ij} \rangle \langle S_{ij} \rangle}, \tag{14}$$

which is based on an unjustified extension of the surface-layer similarity relations to heights well above the surface layer.

In the region of $z > 0.5$ h (h is the ABL height), one can set $\gamma = 1$ and $\nu_T = 0$, because mean-field eddy-viscosity and isotropy factor play important roles only near a bounding surface where mean wind shear is large. For the sake of consistency, a similar correction should be applied to the SGS temperature (or scalar) field. However, Sullivan *et al.* (1994) found that correcting the velocity field also made a substantial improvement in the mean-potential temperature profile. So no additional correction is applied to the expression of the SGS heat flux.

2.3. A PRELIMINARY EVALUATION OF THE TWO SGS MODELS

Simulations of a shear-dominated weakly unstable case and a neutral case are performed with the above mentioned simplified two-part eddy-viscosity first-order SGS model and the Smagorinsky SGS model in TASS-LES. The various input parameters and initial fields are almost the same as in Sullivan *et al.* (1994) and Moeng and Sullivan's (1994) SB1 case. For this case, the domain is 2000 m $\times$ 2000 m $\times$ 750 m and the number of grid points in x, y and z directions are 50 $\times$

50×75, respectively. The initial potential temperature is 300 K below 450 m; it increases by 8 K across the 60 m inversion layer from 450 m to 510 m and further increases with a gradient of 3 K km^{-1} above 510 m. Initially, the wind velocity is in geostrophic balance and a barotropic environment is assumed where geostrophic wind is in x direction ($U_g = 15$ ms^{-1}, $V_g = 0$). The surface heat flux is specified as 0.02 K ms^{-1} and the surface roughness $z_0 = 0.16$ m.

In TASS, the set of grid-volume-averaged equations of motion and thermodynamic energy are solved on an Arakawa-C type mesh. Periodic or open boundary conditions are used in the horizontal direction, while a sponge layer with three grid intervals has been added on the top of the physical domain. At the top boundary, there exists neither heat nor mass transfer. The lower boundary employs a no-slip condition. There is choice of different surface boundary conditions by which one can specify a uniform surface temperature, a uniform heat flux or the surface energy budget. Here, we specified a uniform heat flux at the surface.

The total simulation time for the weakly unstable case is 3.5 h of which the last 60 min are used for obtaining the average statistics. The simulation time is more than 18 times the large-eddy turnover time and large enough for a quasi-steady state to be reached. In order to save spin-up time, the simulation of neutral case is built from the weakly unstable flow simulation. Another 2 h simulation is performed after setting the surface heat flux to zero. The last 60 min of the simulation is used for obtaining averages and other statistics.

Figure 1 shows the profiles of the Monin-Obukhov similarity functions ϕ_m and ϕ_h for the weakly unstable and neutral cases using two SGS models. They are defined as:

$$\phi_m = \frac{kz}{u_*}\left(\left(\frac{\partial U}{\partial z}\right)^2 + \left(\frac{\partial V}{\partial z}\right)^2\right)^{1/2}, \tag{15}$$

$$\phi_h = \frac{kz}{\theta_*}\left(\frac{\partial \Theta}{\partial z}\right), \tag{16}$$

where θ_* is defined by the surface kinematic heat flux Q_0 and the friction velocity u_*:

$$\theta_* = -Q_0/u_*. \tag{17}$$

The results from the surface layer similarity theory are also presented. The empirical forms we used for unstable and neutral conditions are:

$$\phi_m = (1 - 15\zeta)^{-1/4}, \tag{18}$$

$$\phi_h = (1 - 15\zeta)^{-1/2}, \tag{19}$$

where $\zeta = z/L$, and L is the Obukhov length.

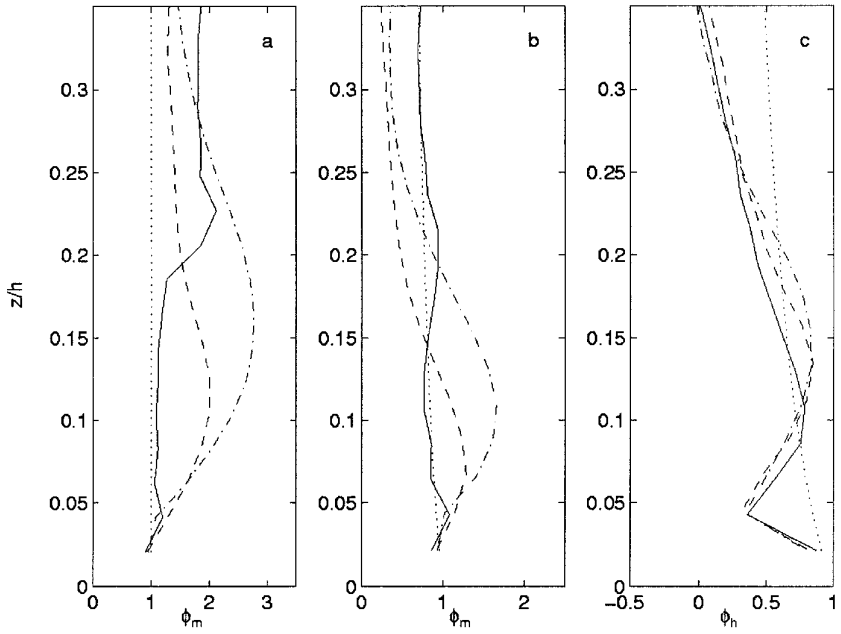

Figure 1. Comparison of simulated and empirical (measured) Monin-Obukhov similarity functions ϕ_m and ϕ_h in the lower part of PBL: (a) neutral case, (b) and (c) weakly-unstable case. Dotted line represents similarity theory, dashed-dot line Smagorinsky model, dashed line the simplified two-part eddy viscosity model, and solid line the proposed SGS model results.

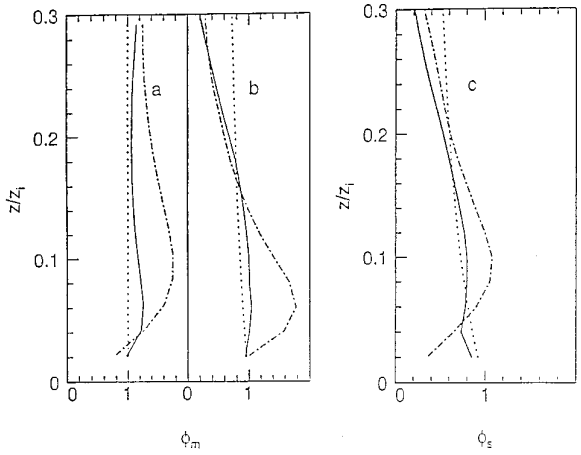

Figure 2. Same as Figure 1, (a) neutral case, (b) and (c) weakly-unstable case, solid line Sullivan *et al.*'s model, dashed-doted line their baseline model, dotted line similarity theory (reprinted after Sullivan *et al.* (1994)).

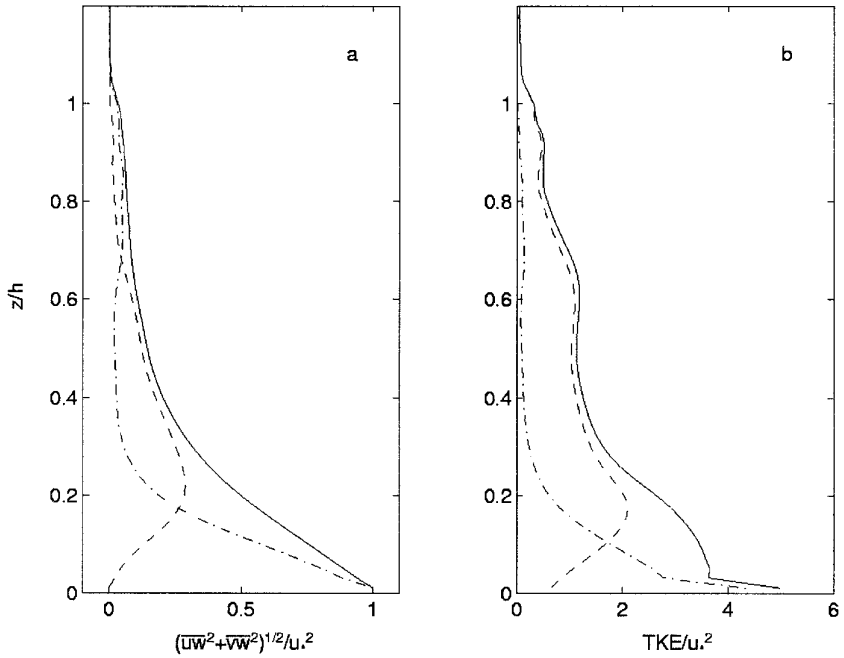

Figure 3. (a) Horizontal momentum flux, and (b) TKE profiles from Smagorinsky model for the neutral case; solid line total, dashed line resolved part, dashed-dot line subgrid part.

The height is non-dimensionalized by the ABL depth h, which is defined as the height where the minimum heat flux occurs. It can be seen that the simplified two-part eddy viscosity model gives an overall better performance than the Smagorinsky model in TASS-LES. It has less deviation from the similarity theory prediction which is expected to be valid only in the surface layer ($z/h \leqslant 0.1$). However, comparing Figure 1 with the corresponding results from Sullivan *et al.* (1994) (Figure 2), we find that the simplified two-part eddy viscosity model did not perform as good as the Sullivan *et al.*'s (1994) two-part eddy viscosity model. The reason may be that the simplified model is a first-order closure as compared to the TKE closure model of Sullivan *et al.* (1994).

Figures 3 and 4 give the TKE and momentum flux profiles for the neutral case using the Smagorinsky's model and the simplified two-part eddy viscosity model. The TKE and momentum flux are non-dimensionalized by u_*^2. It can be noted that the simplified two-part eddy viscosity model gives significantly lower SGS momentum flux and TKE values in the surface layer as compared to the Smagorinsky model. But comparing these with those of Sullivan *et al.* (1994) (not shown here), the simplified model gives somewhat smaller values of momentum flux and TKE. In particular, the momentum flux decreases very rapidly near the surface which is somewhat unphysical. This led us to seek further refinements to

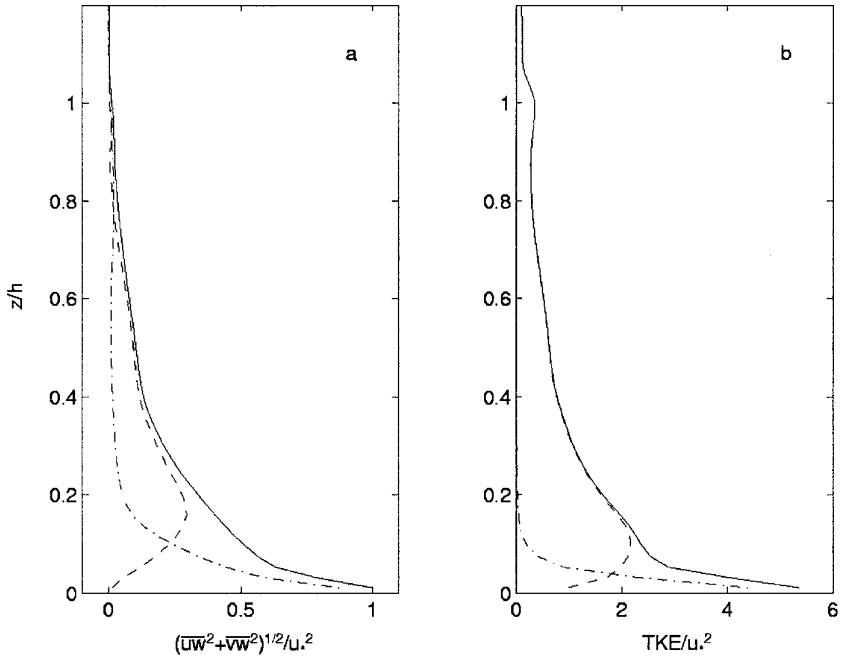

Figure 4. Same as Figure 3, but from simplified two-part eddy viscosity model.

the simplified two-part eddy viscosity model, so that it could be effectively used for the shear-dominated surface layer and the PBL under near-neutral and stable conditions.

2.4. PROPOSED REFINEMENTS TO THE SGS MODEL

Although the simplified two-part eddy-viscosity SGS model represents a noticeable improvement over the Smagorinsky model, further refinements were found necessary for more realistic simulations of neutral and stable boundary layers. The same expression (13) for the mean-field eddy viscosity at the first grid point height z_1 is retained. However, a different expression is obtained for the mean-field eddy viscosity above z_1, but within the lower part of the ABL, because the original expression (14) proposed by Sullivan *et al.* (1994) is limited to only the constant-flux (surface) layer.

In the lower part of the ABL, the resolved part of the momentum flux increases with height and reaches a maximum at some height h_m. For the sake of simplicity, we assume linear profiles for both the total momentum flux and its resolved part. The magnitude of the former decreases while the resolved portion of the momentum flux increases with height (Figure 5). Assuming that these profiles intersect at $z = h_m$, then |AC| and |DE| represent the SGS parts of momentum flux at z_1 and any

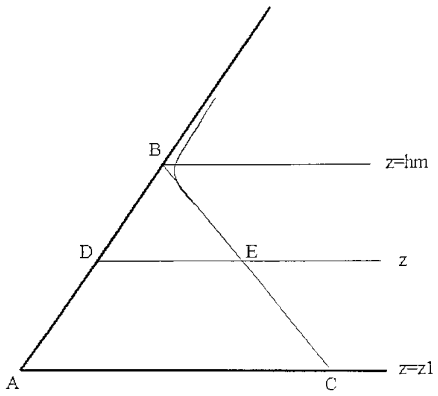

Figure 5. Typical momentum flux profile in the lower part of ABL, heavy line total, light line resolved part.

height z ($z < h_m$), respectively. Applying the gradient transport theory to SGS part of momentum flux:

$$\langle \gamma \nu_t^* \rangle + \nu_T^* = \frac{|AC|}{\left|\frac{\partial V}{\partial z}\right|_{z_1}}, \tag{20}$$

$$\langle \gamma \nu_t \rangle + \nu_T = \frac{|DE|}{\left|\frac{\partial V}{\partial z}\right|_{z}} \quad , \tag{21}$$

where ν_t^* is the fluctuating-field eddy viscosity at the first grid point height z_1. Velocity gradients can be expressed as:

$$\left|\frac{\partial V}{\partial z}\right|_{z_1} = \frac{u_* \phi_m(z_1)}{k z_1}, \tag{22}$$

$$\left|\frac{\partial V}{\partial z}\right|_{z} = \frac{u_{*l} \phi_m(z)}{k z} \quad , \tag{23}$$

where u_{*l} is the local friction velocity, defined as:

$$u_{*l} = \left[(\langle uw \rangle + F_{uw})^2 + (\langle vw \rangle + F_{vw})^2\right]^{1/4}, \tag{24}$$

which can be calculated from the SGS and resolved fluxes from the previous time step. Equation (24) assumes the local similarity scaling in the lower part of the boundary layer, which might be better applicable under stable conditions.

Combining Equations (20), (21), (22) and (23), we have

$$\frac{\langle \gamma \nu_t \rangle + \nu_T}{\langle \gamma \nu_t^* \rangle + \nu_T^*} = \frac{|DE|}{|AC|} \frac{z}{z_1} \frac{\phi_m(z_1)}{\phi_m(z)} \frac{u_*}{u_{*l}}. \tag{25}$$

From the similarity of triangle ABC and DBE, we have

$$\frac{|DE|}{|AC|} = \frac{h_m - z}{h_m - z_1}. \tag{26}$$

Substituting (26) into (25) and assuming $\langle \gamma \nu_t^* \rangle = 0$, it is straightforward to derive the following expression for the mean-field eddy viscosity

$$\nu_T = \nu_T^* \frac{u_*}{u_{*l}} \frac{\phi_m(z_1)}{\phi_m(z)} \frac{(h_m - z)\, z}{(h_m - z_1)\, z_1} - \langle \gamma \nu_t \rangle. \tag{27}$$

Equations (20) and (21) are derived from the horizontal averaging of Equation (8) and assuming $\langle \nu_t S_{ij} \rangle = \langle \nu_t \rangle \langle S_{ij} \rangle$. This assumption neglects the fluctuating components of strain compared to the mean strain. Theoretically, we have

$$\langle \nu_t S_{ij} \rangle = \langle \nu_t \rangle \langle S_{ij} \rangle + \langle \nu_t' S_{ij}' \rangle. \tag{28}$$

Defining $\beta = \langle \nu_t' S_{ij}' \rangle / \langle \nu_t \rangle \langle S_{ij} \rangle$, which is the ratio of two terms on the right-hand side of Equation (28), we find that β is nearly zero at the first grid level z_1. But it could be as large as 0.2 when z is between z_1 and h_m. Then, $\langle \nu_t S_{ij} \rangle = (1 + \beta) \langle \nu_t \rangle \langle S_{ij} \rangle$, so that, Equation (27) should be modified as

$$\nu_T = \nu_T^* \frac{u_*}{u_{*l}} \frac{\phi_m(z_1)}{\phi_m(z)} \frac{(h_m - z)\, z}{(h_m - z_1)\, z_1} - (1 + \beta) \langle \gamma \nu_t \rangle. \tag{29}$$

This expression of the mean-field eddy viscosity is used in our proposed model; it differs from Equation (14) used by Sullivan *et al.* (1994).

3. Simulation Results for Neutral and Slightly Unstable Cases

3.1. MONIN–OBUKHOV SIMILARITY FUNCTIONS

The proposed (refined) SGS model in Section 2.4 (hereafter, referred as proposed SGS model) is used to rerun the two simulations mentioned in Section 2.2. All parameters and simulation time are the same. Figure 1 shows that the results from the proposed SGS model (solid line) represent substantial improvement over the other two SGS models – the Smagorinsky's model (dashed-dot line) and the simplified two-part eddy viscosity model (dashed line). The excessive mean-wind shear in the surface layer is reduced significantly and a good agreement with the empirical similarity functions extends to about 0.2 h, where h is the PBL height which is assumed equal to the height of inversion base. Although no modifications are made for the corresponding heat diffusivity, the computed ϕ_h profile also has better agreement with the empirical one within $z < 0.2$ h. This shows that the modification to momentum eddy diffusivity also results into significant improvement in the potential temperature profile. Still, ϕ_h is significantly underestimated by the model in the middle part of the surface layer, which may be due to the coarse resolution (grid spacing) used in the model. Additional refinement of the SGS eddy diffusivity of

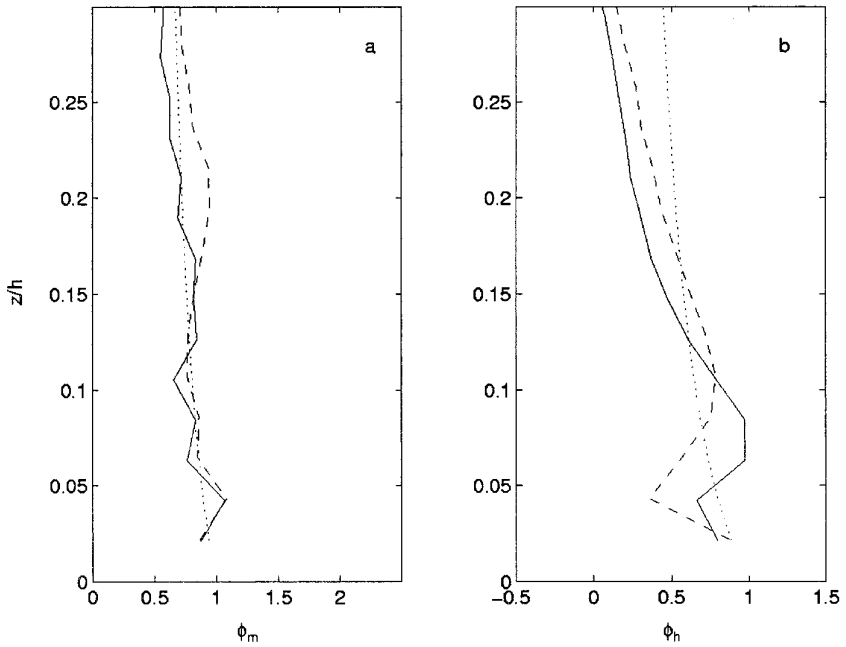

Figure 6. Monin–Obukhov similarity functions ϕ_m and ϕ_h in the lower part of PBL for the weakly unstable case using proposed SGS model with different grid resolutions, (a) ϕ_m and (b) ϕ_h, solid line finer grid resolution, dash line coarse grid resolution, dot line similarity theory.

heat, similar to that done in Part II for the stable cases, is expected to result in a better simulation of ϕ_h and, hence, the temperature profile near the surface.

3.2. GRID RESOLUTION EFFECT

In order to study the grid resolution effect, several simulations with the larger number of grid points ($100 \times 100 \times 75$) were performed using the proposed SGS model and Smagorinsky model. The same domain size was kept, but the grid resolution in horizontal directions was increased by reducing Δx from 40 m to 20 m. All other parameters had the same values as before.

From the results of the proposed (refined) SGS model shown in Figure 6, nondimensional wind shears (ϕ_m) with different grid resolutions are almost the same below 0.15 h and above this height the simulation with finer grid resolution resulted into smaller ϕ_m values. Thus, the proposed SGS model simulates the wind profile and wind shears in the surface layer which are consistent with the M–O similarity theory and not very sensitive to grid resolution. There are larger differences in the simulated potential temperature gradients or ϕ_h in the surface layer between fine and coarse grid resolutions. The height where the maximum potential tem-

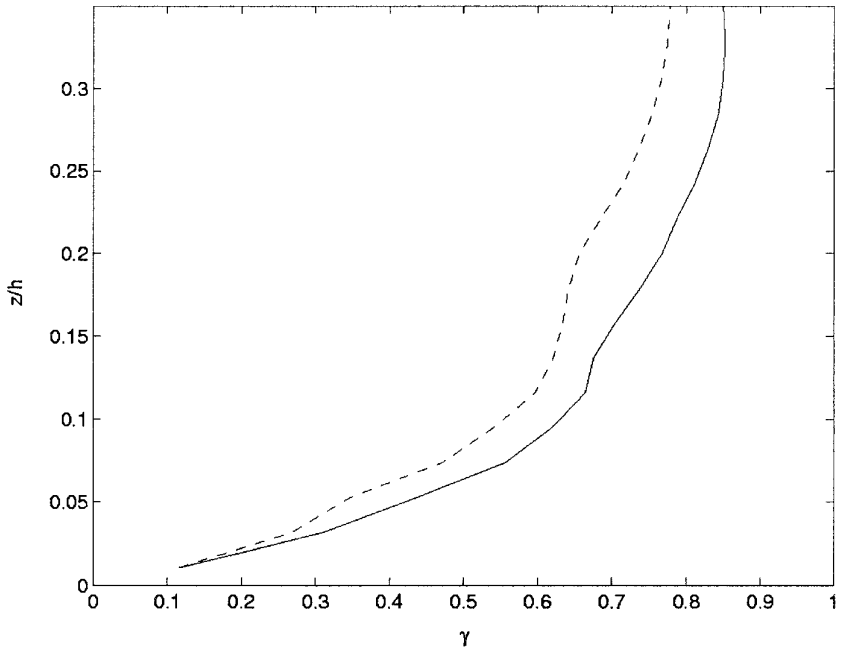

Figure 7. The isotropy factor profiles for different grid resolutions, solid line fine grid resolution, dashed line coarse grid resolution.

perature gradient or ϕ_h occurs decreases with increased grid resolution while the deviation from the empirical similarity function decreases in the lower part of the surface layer. This suggests that the effect of grid resolution is stronger on the mean potential temperature profile than on the mean wind profile, probably due to no modification to the SGS heat diffusivity. Note that the empirical ϕ_m and ϕ_h functions may not be appropriate for $z/h > 0.1$, where h is the PBL height.

Figure 7 shows the variation of isotropy factor γ with normalized height for different grid resolutions using the proposed SGS model. Because the simulation with finer grid resolution can resolve much smaller scale eddies, the value of $\langle S \rangle$ in Equation (9), or the magnitude of the horizontally-averaged deformation tensor decreases and S' increases. From the definition of γ, the isotropy factor increases with increasing grid resolution. All these effects of grid resolution are similar to the results obtained by Sullivan *et al.* (1994). Figure 7 also shows γ increasing with height very rapidly in the surface layer and gradually above that; it has been set equal to one for $z/h \geq 0.5$.

3.3. MOMENTUM FLUX AND TKE PROFILES

Figure 8 shows the momentum flux and TKE profiles from the simulations of the proposed model for neutral case. Obviously, compared with the Smagorinsky

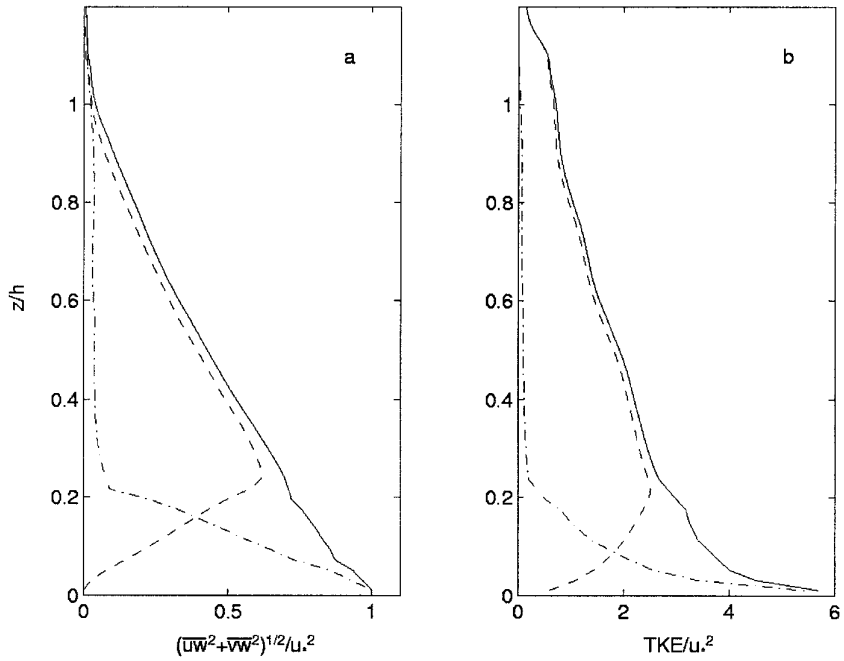

Figure 8. (a) Horizontal momentum flux, and (b) TKE profiles from the proposed SGS model for the neutral case; solid line total, dashed line resolved part, dashed-dot line subgrid part.

model results shown in Figure 3, the resolved part is enlarged and the ratio of the subgrid scale part to the resolved part is reduced in the proposed SGS model. This is the expected result and in good agreement with Sullivan *et al.* (1994). Note that the total momentum flux profile becomes closer to linear in the proposed model.

The total TKE/u_*^2 is increased in the proposed model. Near the ground, the maximum value of $\mathrm{TKE}/u_*^2 \approx 5.8$ is more consistent with the observations of turbulence in the neutral surface layer (Stull, 1988). Further, comparing the results of simulation of weakly unstable case by the two models (not shown), we find that the resolved part of the normalized TKE in the surface layer for weakly unstable case was larger than that for neutral case. This is expected from the additional generation of TKE due to the buoyant production as a result of surface heating in the weakly unstable case.

3.4. SPECTRAL ANALYSIS

Figure 9 shows the computed spectra of stream-wise velocity, cross-stream velocity and vertical velocity from both the Smagorinsky model and our proposed SGS model for three different heights in the lower part of the neutral ABL. The straight line with $-\frac{5}{3}$ slope from the inertial sub-range hypothesis is also presented. It can

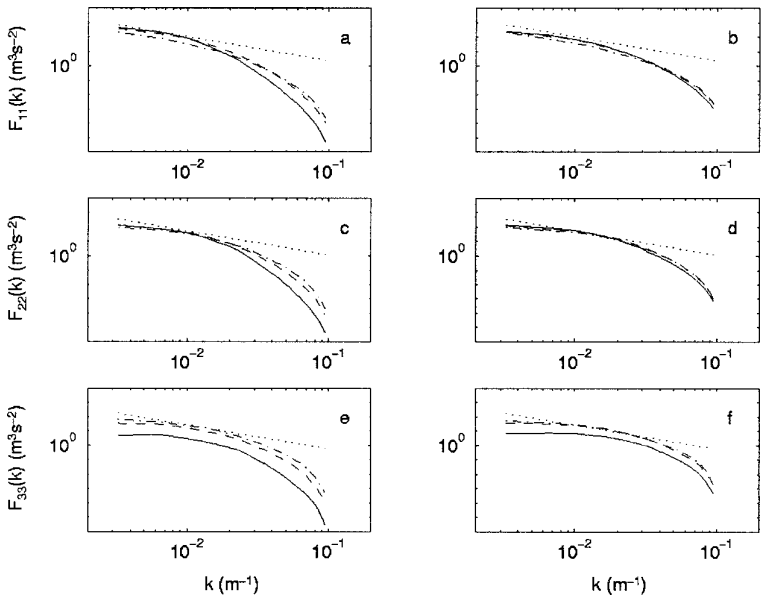

Figure 9. Spectra of stream-wise velocity, cross stream-wise velocity and vertical velocity from different SGS models. (a), (c) and (e) Smagorinsky model, (b), (d) and (f) proposed SGS model; solid line $z \approx 0.1$ h, dash line $z \approx 0.2$ h, dashed-dot line $z \approx 0.4$ h, dot line $-\frac{5}{3}$ slope line.

be seen that the proposed SGS model produces a more extensive inertial sub-range than that produced by the Smagorinsky model (simulated spectra may also depend on the value of Smagorinski constant). Especially, the spectral slopes at large wave numbers are less steep and the energy dissipation by the small scale eddies is reduced. This improvement is also achieved by Kosovic (1997) using a nonlinear SGS model which works only in neutral and stable conditions. It is well known that due to the limited grid resolution, calculated spectra of turbulence from LES can not match the very extensive inertial sub-ranges found in the measured spectra of atmospheric turbulence in unstable and neutral ABLs (Stull, 1988).

3.5. VISUALIZATION OF THE FLOW PATTERN

Figures 10 and 11 give the plots of u and w contours in the x–y plane and the x–z section at a specified time using the Smagorinsky model and the proposed SGS model for the neutral case. The contour plots in the x–y plane are at the height about 0.2 h. While the plots in the x–z section are along the middle line in y direction. Comparing the results from the two SGS models, we find they generate roughly similar flow patterns. But the proposed SGS model clearly shows more three-dimensional flow structures, while u and w contours in x–y plane from the Smagorinsky model show more elongated structures aligned with the mean wind

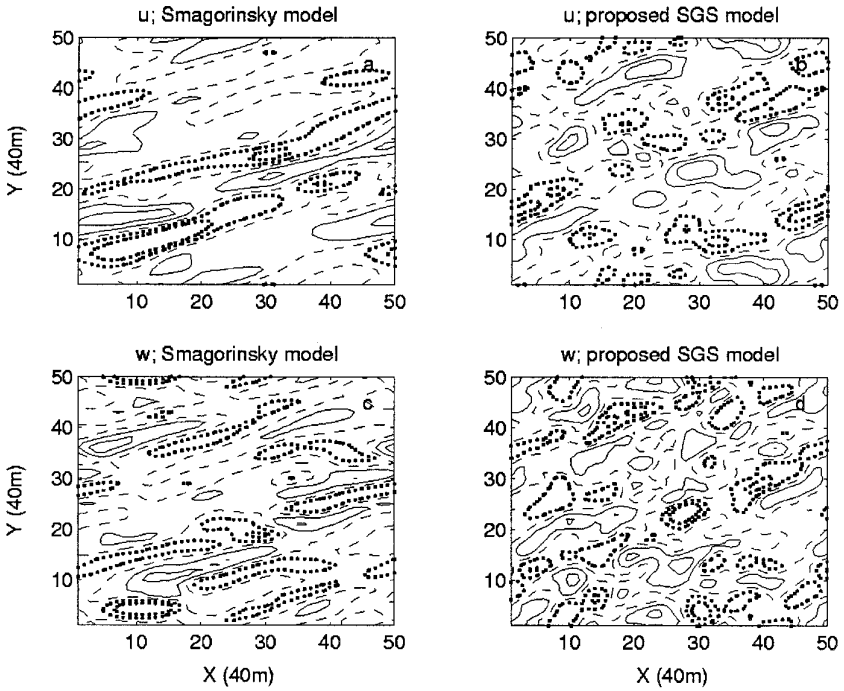

Figure 10. Contours of u and w in the x–y plane at $z \approx 0.2$ h from different SGS models. (a) and (c) Smagorinsky model; (b) and (d) proposed SGS model; (a) and (b) u contours; (c) and (d) w contours; dot line negative value, dash line 0, solid line positive value.

which was first found by Mason and Thomson (1987). Similar flow patterns were also observed by Sullivan *et al.* (1994) using their baseline model and two-part eddy viscosity model. Although the results from our proposed SGS model still have the same streaky structure, they are not very elongated and their alignments are not so striking either.

On the other hand, differences in the structures seen in the x–z section plots of u and w contours from the two models are more subtle. The proposed SGS model generated stronger turbulent motions reflecting the enhancement of the resolved part of TKE.

4. Conclusions

In the region near the ground where subgrid scale (SGS) motions are more important, the results of LES become very sensitive to detailed characteristics and parameterizations of SGS model. The traditional Smagorinsky model gives an excessive mean wind shear and the mean wind profiles differ from those observed and predicated by the Monin-Obukhov similarity theory. Sullivan *et al.* (1994) developed a two-part SGS eddy viscosity model to improve the simulations in the

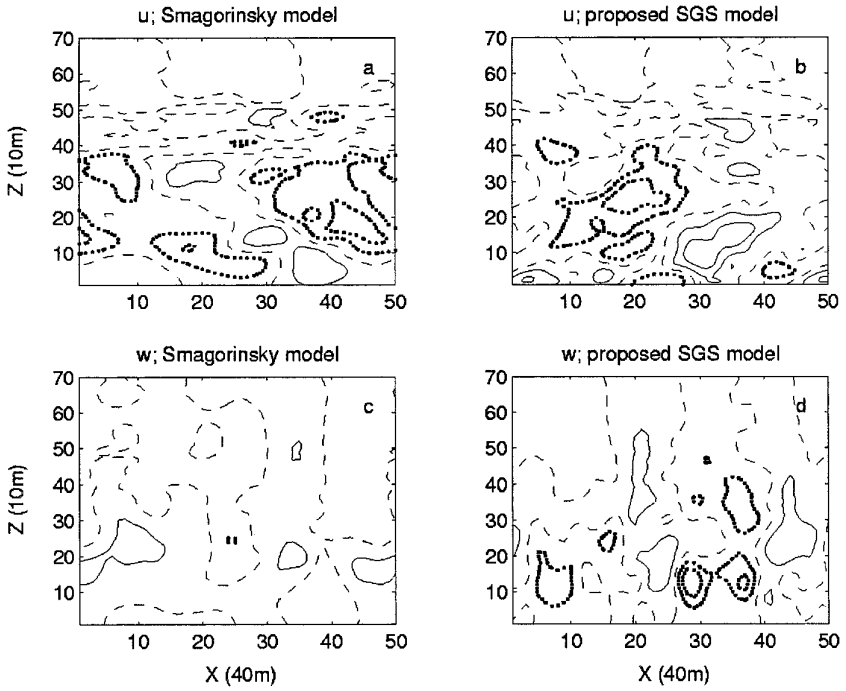

Figure 11. Same as Figure 10, but in the x–z section along the middle line of y direction. (a) and (b) u contours; (c) and (d) w contours; dot line negative value, dash line 0, solid line positive value.

near-wall region. A simplified form of their model was also used in the TASS-LES model which originally used a modified Smagorinsky first-order closure. Although mean wind shears near the surface are significantly reduced by using the simplified two-part eddy viscosity model, the results are still not as good as those from the original Sullivan *et al.*'s (1994) SGS model with the TKE closure scheme. Thus, a refined SGS model is proposed based on Sullivan *et al.*'s (1994) two-part eddy viscosity model. The same expression for the mean-field eddy viscosity at the first grid point height is still used. However, a different expression is obtained for the mean-field eddy viscosity above the first grid point height, but within the lower part of the ABL.

A series of simulations have been performed to test the proposed SGS model. For both the shear-dominated weakly unstable case and the neutral case with initial strong wind shear, the proposed SGS model essentially reduces the excessive wind shear near the ground and well simulates the surface-layer similarity profiles. The SGS portions of momentum flux and TKE are noticeably reduced, and correspondingly the resolved portions are enhanced. The results of spectral analysis also show that the energy dissipation due to small scale eddies is also reduced compared with the results from the original Smagorinsky model in the TASS-LES.

Acknowledgements

We want to express our thanks to North Carolina Supercomputer Center for using its CRAY facility. The partial support of the Cooperative Agreement No. NCC-1-188 with NASA-Langley is also gratefully acknowledged.

References

A. Andren, The structure of stably stratified atmospheric boundary layers: A large- eddy simulation study . *Quart. J. Roy. Meteorol. Soc.* **121** (1995) 961–985.

A. Andren, A. Brown, J. Graf, C.H. Moeng, P.J. Mason, F.T. Nieuwstadt and U. Schumann, A larger-eddy simulation of neutrally stratified boundary layers: A comparison of four computer codes. *Quart. J. Roy. Meteorol. Soc.* **120** (1994) 1457–1484.

S.P. Arya, *Air Pollution Meteorology and Dispersion*, Oxford University Press, Oxford (1999) 310 pp.

J.W. Deardorff, A three-dimensional numerical investigation of idealized planetary boundary layer. *Geophys. Fluid Dyn.* **1** (1970) 377–410.

J.W. Deardorff, Three-dimensional numerical modeling of the planetary boundary layer. In: D.A. Haugen (ed.), *Workshop on Micrometeorology*, American Meteorological Society, Boston, MA (1973) pp. 271–311.

D.S. DeCroix, Y.-L. Lin and D. G. Schowalter, Cellular convection embedded in the convective planetary boundary layer surface layer, *J. Wind. Eng. Ind. Aerodyn.* **66 & 67** (1997) 387–401.

B. Kosovic, Subgrid-scale modeling for the large-eddy simulation of high- Reynolds-number boundary layers. *J. Fluid Mech.*, **336** (1997) 151–182.

P.J. Mason, Large-eddy simulation of the convective atmospheric boundary layer. *J. Atmospheric. Sci.* **46** (1989) 1492–1516.

P.J. Mason, Large-eddy simulation: A critical review of the technique. *Quart. J. Roy. Meteorol. Soc.* **120** (1994) 1–26.

P.J. Mason and D.J. Thomson, Large-eddy simulations of the neutral-static-stability planetary boundary layers. *Quart. J. Roy. Meteorol. Soc.* **113** (1987) 413–443.

P.J. Mason and D.J. Thomson, Stochastic backscatter in large-eddy simulations of boundary layers. *J. Fluid Mech.* **242** (1992) 51–78.

C.-H. Moeng, A large-eddy simulation model for the study of planetary boundary layer. *J. Atmospheric. Sci.* **41** (1984) 2052–2062.

C.-H. Moeng and P.P. Sullivan, A comparison of shear and buoyancy driven planetary boundary-layer flows. *J. Atmospheric. Sci.* **51** (1994) 999–1022.

F.T.M. Nieuwstadt and R.A. Brost, The decay of convective turbulence. *J. Atmospheric. Sci.* **43** (1986) 532–546.

F.H. Proctor, The Terminal Area Simulation System, Volume I: Theoretical formulation. NASA Contractor Report 4046 DOT/FAA/PM-86/50, (1987) I.

F.H. Proctor, Numerical simulation of an isolated microburst. Part I: Dynamics and structure. *J. Atmos. Sci.* **45** (1988) 3137–3159.

D.G. Schowalter, D.S. DeCroix, Y.-L. Lin, F.H. Proctor, S.P.S. Arya and M.L. Kaplan, Turbulent statistics in the atmospheric boundary layer: A comparison of large-eddy simulation with observations, *11th Symposium on Boundary Layers and Turbulence*, Boston, MA (1995) pp. 552–555.

D.G. Schowalter, D.S. DeCroix, Y.-L. Lin, S.P.S. Arya and M.L. Kaplan, Planetary boundary layer simulation using TASS. NASA Contractor Report 198325, NASA Langley Research Center, Hampton, VA (1996a) 34 pp.

D.G. Schowalter, D.S. DeCroix, Y.-L. Lin, S.P.S. Arya and M.L. Kaplan, The sensitivity of large-eddy simulation of local and non-local drag coefficients at the lower boundary. NASA Contractor Report 198310, NASA Langley Research Center, Hampton, VA (1996b) 36 pp.

U. Schumann, Subgrid scale model for finite difference simulations of turbulent flows in plane channels and annuli, *J. Comp. Phys.* **18** (1975) 376–404.

J. Smagorinsky, General circulation experiments with the primitive equations, Part I: The basic experiment. *Mon. Weath. Rev.* **91** (1963) 99–152.

R.B. Stull, *An Introduction to Boundary Layer Meteorology*, Kluwer Academic Publishers, Dordrecht (1988) 666 p

P.P. Sullivan, J.C. McWilliams and C.-H. Moeng, A subgrid-scale model for large-eddy simulation of planetary boundary layer. *Bound.-Layer Meteorol.* **71** (1994) 247–276.